Dalton Transactions

PAPER

View Article Online
View Journal | View Issue

Cite this: *Dalton Trans.*, 2015, **44**, 1700

Neutral diiron(III) complexes with $Fe_2(\mu\text{-}E)_2$ (E = O, S, Se) core structures: reactivity of an iron(I) dimer towards chalcogens†

Lea Fohlmeister,[a] Kuduva R. Vignesh,[b,c] Florian Winter,[d] Boujemaa Moubaraki,[a] Gopalan Rajaraman,[b] Rainer Pöttgen,[d] Keith S. Murray[a] and Cameron Jones*[a]

Received 7th October 2014,
Accepted 20th November 2014

DOI: 10.1039/c4dt03081h

www.rsc.org/dalton

Three neutral bis(μ-chalcogenido)diiron(III) complexes, [{(*N*,*N*′-Pipiso)Fe(μ-E)}$_2$] (Pipiso$^-$ = [(DipN)$_2$C(*cis*-2,6-Me$_2$NC$_5$H$_8$)]$^-$, (Dip = C$_6$H$_3$Pr$^i_2$-2,6; E = O, S or Se) have been prepared by reactions of the iron(I) dimer [{(μ-*N*,*N*′-Pipiso)Fe}$_2$] with O_2, S_8 or Se_∞. Treating the μ-selenido compound [{(*N*,*N*′-Pipiso)Fe-(μ-Se)}$_2$] with O_2 cleanly generated its μ-oxo counterpart, [{(*N*,*N*′-Pipiso)Fe(μ-O)}$_2$]. X-ray crystallographic analyses of the compounds showed them to possess $Fe_2(\mu\text{-}E)_2$ core structures with distorted square planar (E = O) or tetrahedral (E = S or Se) iron coordination geometries. Magnetic, ^{57}Fe Mössbauer spectroscopic and computational studies indicate medium to strong antiferromagnetic coupling between the two high-spin Fe^{III} ions in all three compounds.

Introduction

Bis(μ-chalcogenido) diiron core structures, $Fe_2(\mu\text{-}E)_2$ (E = O or S), with the iron centres in variable oxidation states, are thought to play important roles in the active sites of a number of metalloenzymes found in nature. For example, $Fe_2(\mu\text{-}O)_2$ core motifs have been proposed for intermediates in the catalytic cycles of methane monooxygenases (MMOs), which catalyse the oxidation of methane with O_2 to yield methanol, and ribonucleotide reductases (RNRs), which are responsible for the *de novo* synthesis of deoxyribonucleotides.[1,2] In addition, $Fe_2(\mu\text{-}S)_2$ units are present in [2Fe–2S] clusters at the core of ferredoxins and Rieske-type proteins.[3] These proteins are important to a number of biological processes, which include electron transport, respiration and photosynthesis. It is of note that the $Fe_2(\mu\text{-}S)_2$ cores of some ferredoxins can be readily substituted with $Fe_2(\mu\text{-}Se)_2$ units, thereby aiding the study of the active sites of those proteins.[4]

A considerable number of molecular model complexes of all of the above mentioned proteins have been prepared in the laboratory.[2–4] However, structurally characterized neutral complexes with four-coordinate iron centres are rare, and are, in fact, unknown for the $Fe_2(\mu\text{-}O)_2$ core. We have recently reported on the unusual guanidinate bridged, three-coordinate iron(I) dimer, **1** (Chart 1), which exhibits the shortest known Fe–Fe bond (2.1270(7) Å).[5] Given the highly reactive nature of this compound, and its extremely bulky ligands, we proposed that its reaction with elemental chalcogens could give rise to low-coordinate iron chalcogenide dimers, possibly containing

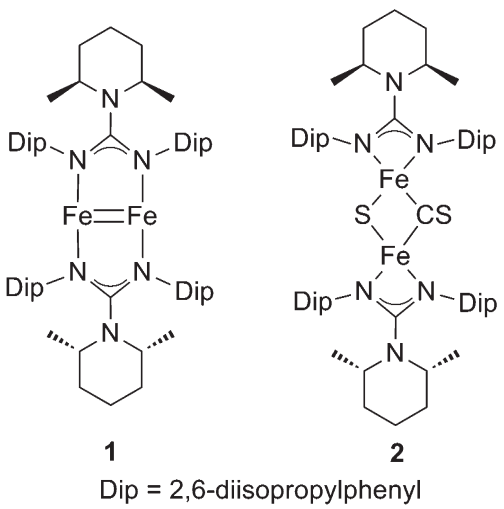

1 **2**

Dip = 2,6-diisopropylphenyl

Chart 1

[a]*School of Chemistry, Monash University, P.O. Box 23, Melbourne, Victoria 3800, Australia. E-mail: cameron.jones@monash.edu*
[b]*Department of Chemistry, Indian Institute of Technology Bombay Powai, Mumbai 400076, India*
[c]*IITB-Monash Research Academy, IIT Bombay, Mumbai 400076, India*
[d]*Institut für Anorganische und Analytische Chemie, Corrensstraße 30, D-48149 Münster, Germany*

†Electronic supplementary information (ESI) available: Crystallographic data as CIF files for all crystal structures; further details of the spectroscopic, crystallographic, magnetochemical, and computational studies. CCDC 1009399–1009401. For ESI and crystallographic data in CIF or other electronic format see DOI: 10.1039/c4dt03081h

$Fe_2(\mu\text{-}E)_2$ structural cores. Some support for this proposal came from our recent report of the reaction of **1** with CS_2, which yields the square planar iron(II) μ-sulfide complex, **2**.[6] Herein, we show that reactions of **1** with several chalcogens do, indeed, lead to the four-coordinate, bis(μ-chalcogenido) complexes, [{(*N*,*N*′-Pipiso)Fe(μ-E)}$_2$] (Pipiso$^-$ = [(DipN)$_2$C(*cis*-2,6-$Me_2NC_5H_8$)]$^-$, (Dip = $C_6H_3Pr^i_2$-2,6; E = O, S or Se), the magnetic, spectroscopic, structural and bonding properties of which have been explored.

Results and discussion

Treating hexane solutions of **1** with an excess of dry O_2 or N_2O led to good isolated yields of the bis(μ-oxo) iron(III) complex, **3**, as an orange-brown crystalline solid upon work-up (Scheme 1). Similarly, reactions of toluene solutions of **1** with S_8 or grey selenium (Se_∞) afforded low to moderate isolated yields of the bis(μ-chalcogenido) iron(III) dimers, dark red-brown **4** and dark brown **5**, respectively. Intriguingly, exposing d_6-benzene solutions of **5** to atmospheres of dry O_2 rapidly, and quantitatively, generated the oxide **3** (and presumably elemental selenium), as determined by ^{1}H NMR spectroscopy. In contrast, solutions of **5** are unreactive towards N_2O. For sake of comparison, compound **4** was also treated with an excess of dry O_2, though this did not yield **3**, and instead gave a mixture of products which could not be purified or identified. Considering that we have previously shown the coordination properties, and steric profile, of bulky guanidinates (*e.g.* Pipiso) to be similar to those of bulky β-diketiminate (Nacnac) ligands,[7] the formations of **3** and **4** should be compared to related reactions of "masked (Nacnac)Fe^I" complexes with Me_3NO and S_8. Instead of iron(III) chalcogenide products, Holland and co-workers have reported these reactions to yield mono(μ-chalcogenido) iron(II) complexes, [{(Nacnac)Fe}$_2$(μ-E)] (E = O[8] or S[9]). With that said, sub-stoichiometric quantities of the chalcogen source were used in these reactions, and the reactivity of [{(Nacnac)Fe}$_2$(μ-E)] towards excess chalcogen was not reported.

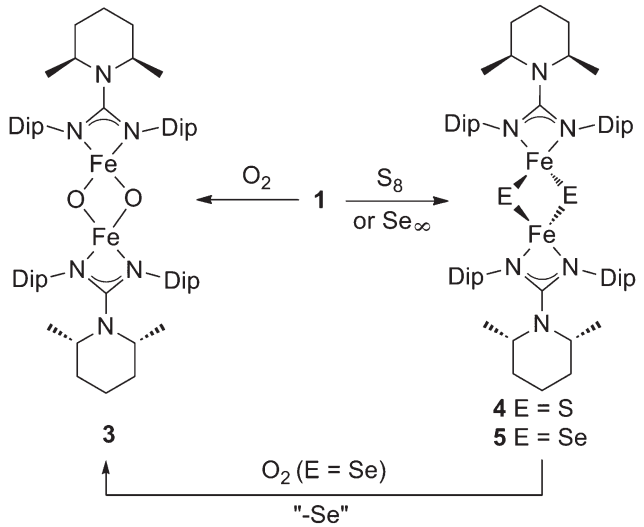

Scheme 1 Preparation of compounds **3**–**5**.

The solid state structures of **3**–**5** were determined by X-ray crystallographic analyses. Those for **3** and **4** are shown in Fig. 1 (see also Table 1), while the molecular structure of **5**, which is isomorphous to **4**, can be found in the ESI.† The two iron(III) centres of compound **3** are chelated by delocalized guanidinate ligands, in addition to being essentially symmetrically bridged by two oxide ligands, to give the molecule a four-membered Fe_2O_2 ring at its core. While a handful of related six-coordinate cationic complexes bearing $Fe_2(\mu\text{-}O)_2$ cores have been reported,[2] as far as we are aware, compound **3** is the first neutral example, and the only four-coordinate representative. In addition, the coordination geometry at the iron centres is distorted square planar ($\sum$ of angles around Fe(1) = 359.99°, dihedral angle between NFeN and OFeO least squares planes = 0.76°), which is rare for iron(III),[10] and contrasts to the tetrahedral iron coordination in **4** and **5** (see below). It should be noted, however, that in the crystal of **3** chosen for the diffraction experiment, there is a small amount of disorder of the atomic positions of the oxide ligands. Consequently, it can be viewed as a co-crystal of its square planar and tetrahedral

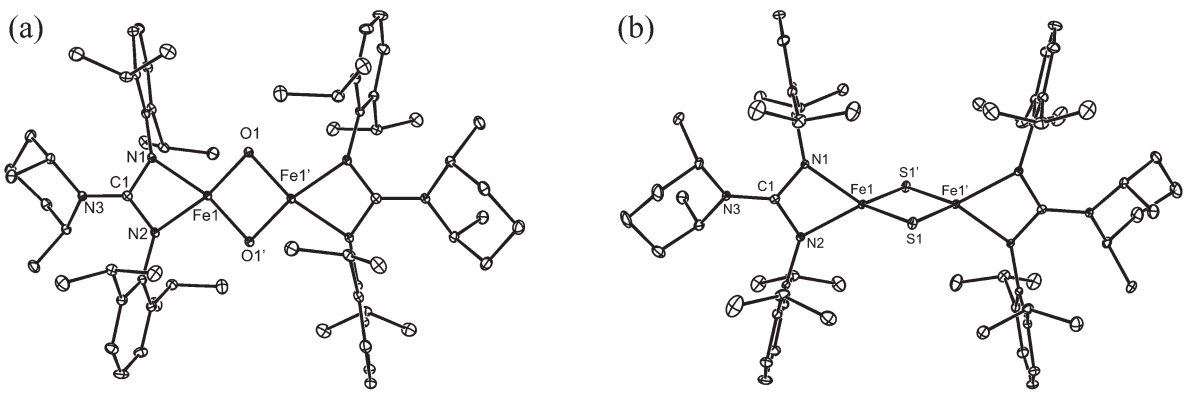

Fig. 1 Displacement ellipsoid plots (25% probability surface) of the molecular structures of (a) **3** and (b) **4**. Hydrogen atoms are omitted. Selected metrical parameters are given in Table 1 (see ESI† for the molecular structure of **5**).

Table 1 Selected interatomic distances (Å) and angles (°) for **3–5** (E = O, S or Se)

	3	4	5
Fe(1)–E(1)	1.773(2)	2.1831(9)	2.3095(7)
Fe(1)–E(1)′	1.791(2)	2.1824(9)	2.3103(10)
Fe(1)–N(1)	1.977(2)	2.008(2)	2.014(2)
Fe(1)–N(2)	1.965(2)	2.012(2)	2.016(2)
Fe(1)···Fe(1)′	2.475(1)	2.647(1)	2.734(1)
E(1)–Fe(1)–E(1)′	92.03(8)	105.35(3)	107.44(3)
Fe(1)–E(1)–Fe(1)′	87.97(8)	74.65(3)	72.56(3)
N(1)–Fe(1)–N(2)	67.11(8)	66.18(9)	66.27(7)

forms, which are present in an approximate ratio of 92 : 8 (see ESI† for further details).

The Fe–O distances in **3** are significantly shorter than those in all cationic bis(μ-oxo)diiron(III) complexes (range: 1.805–1.935 Å),[2] presumably as a result of the lower iron coordination number in the compound. Moreover, these distances are markedly shorter than all previously reported Fe–OH separations,[11] which rules out the presence of hydroxide ligands in **3**. In addition, the O···O separation in the compound (2.564(2) Å) is well outside the range found for bridging peroxide ligands,[11] and therefore there can be no O–O bond in the compound. The Fe(1)···Fe(1)′ distance in **3** (2.475(1) Å, *cf.* 2.5800(6) Å in **2**[6]) is notably shorter than all similar separations in cationic bis(μ-oxo)diiron(III) compounds (range: 2.683–2.792 Å[2]), and although it is well within the sum of the covalent radii for two iron centres (2.64 Å[12]), it is unlikely that there is any significant bonding interaction between the atoms. It is interesting to note, however, that the Fe···Fe distance in **3** is similar to that determined (*ca.* 2.46 Å) from an experimental EXAFS analysis of the higher oxidation state $Fe^{IV}_2(\mu\text{-}O)_2$ core proposed for intermediate *Q* of methane monooxygenase (MMO).[2e] With that said, a more recent computational study has questioned the results of that experimental study, and points towards an Fe···Fe separation of 2.84 Å for MMO intermediate Q.[2g]

Compounds **4** and **5** are isostructural, and unlike square planar **3**, they possess distorted tetrahedral iron coordination geometries. The Fe–E bond lengths and Fe–E–Fe angles in the compounds lie within the known ranges for tetrahedral diiron complexes containing $Fe_2(\mu\text{-}E)_2$ cores, of which there are quite a few examples in the literature.[3,11] Not surprisingly, their Fe···Fe separations (**4**: 2.647(1) Å, **5**: 2.734(1) Å) are greater than that in **3**, which reflects the larger chalcogenide ligands in the compounds. As was the case for **3**, the bond distances within the chelating NCN backbones of the guanidinate ligands imply electronic delocalization over those fragments.

While it might be expected that the signals in the solution state ^{1}H NMR spectra of the, presumably, high-spin iron(III) complexes, **3–5**, should be significantly paramagnetically shifted, this does not appear to be the case, indicative of strong antiferromagnetic coupling. Although the signals are broadened, for all compounds they are found in the range δ 0–10 ppm, and the spectral patterns are largely consistent with the observed solid state structures. The solution state UV/visible spectra were also recorded for **3** and **4** (see ESI†). Of most interest is that for **4** which exhibits three absorption maxima at λ_{max} = 595 (1913 L mol^{-1} cm^{-1}), 504 (2543 L mol^{-1} cm^{-1}) and 353 (8080 L mol^{-1} cm^{-1}) nm. It is noteworthy that three LMCT bands at similar wavelengths are typically found for Rieske-type proteins in their oxidized forms (*i.e.* Fe^{III}/Fe^{III}).[13] In addition, the UV/visible spectrum of **4** is comparable to those of systems that are models for [2Fe–2S] clusters.[14] It is worthwhile mentioning that a number of attempts were made to investigate the solution state electrochemistry of complexes **3** and **4**. These were, however, not successful as the highly reactive compounds were not stable, even under rigorously anaerobic and moisture free conditions, in the presence of a range of supporting electrolytes. These included the perfluoroaluminate salt, $[NBu^n_4][Al\{OC(CF_3)_3\}_4]$, which is normally considered to be of very low reactivity.[15]

The magnetic properties of **3–5** were investigated in both the solution and the solid states. In solution (d_6-benzene), low magnetic moments were reproducibly recorded for **3** and **4** (μ_{eff} = 1.8(1) μ_B and 1.3(1) μ_B per dimer, Evans method), while no magnetic moment was distinguishable for **5** using the Evans method. These observations are consistent with the mildly paramagnetically affected ^{1}H NMR spectra of the compounds, and could indicate strong antiferromagnetic coupling between two high-spin (h.s.) Fe^{III} centres in each compound. In order to investigate this possibility in more detail, variable temperature solid state magnetic susceptibility measurements of **3–5** were carried out. Those for **3** (Fig. 2(a)), surprisingly, revealed a reproducible, and significantly higher, magnetic moment (μ_{eff} = 3.4 μ_B) at 300 K, than was determined in solution. This is, however, itself markedly lower than the theoretical value for two non-interacting h.s. iron(III) centres (μ_{SO} = 8.4 μ_B per two Fe centres). The experimental magnetic moment showed minimal field dependence at low temperatures, indicating no substantial contamination by magnetisable impurities. The magnetic moment decreased steadily until *ca.* 2.0 μ_B at 20 K, then dropped off sharply from 20–2 K. A plot of $\chi_M T$ *vs.* *T* for **3** (Fig. 2(b)) showed similar behaviour. This is quite unusual for h.s. iron(III) centres with bridging oxide ligands, as χ_M should decrease to zero at 0 K, because of population of the S = 0 ground state that derives from a S = 5/2 antiferromagnetically coupled dimer. The experimental χ_M values do not approach zero at low temperatures, possibly indicating the presence of small amounts of an unknown magnetic impurity that becomes almost diamagnetic at 2 K. Attempts were made to fit the μ_{eff} (and $\chi_M T$; note that 8 $\chi_M T = \mu_{eff}^2$) data to an S = 5/2 dimer model (spin Hamiltonian $H = -2J\mathbf{S_1}\cdot\mathbf{S_2}$) that includes 10% of an S = 5/2 monomer impurity contribution to χ_M. The region from T = 300 to 120 K can be fitted well to the parameters g = 2.1, J = −145 cm^{-1}, but this does not reproduce the 2–120 K region, which would show the Curie-like monomer contribution ($\chi_M T$ independent of T). Possible ways to simulate μ_{eff} (and $\chi_M T$) decreasing towards zero between 120 and 2 K would be to include (i) temperature independent paramagnetism, Nα (TIP); but this second-order Zeeman term is zero for h.s. Fe^{III} (ii) zero field splitting in the h.s. monomer impurity

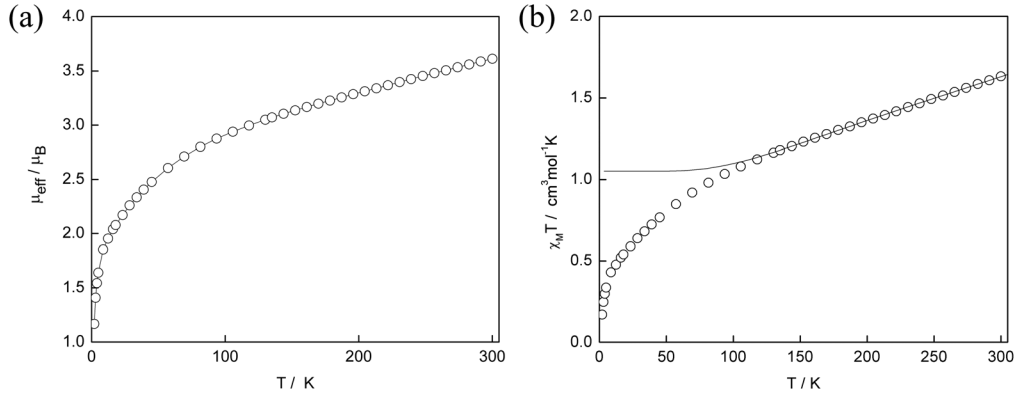

Fig. 2 Plot of (a) μ_{eff} (per two Fe centres) *vs.* *T* for **3**, in an applied field of 1 T (the solid line is a guide to the eye) and (b) $\chi_M T$ (per two Fe centres) *vs.* *T* for **3** (open circles). The solid line is that calculated for an S = 5/2 dimer model using the parameters: g = 2.1, J = –145 cm^{-1} and 10% monomer impurity. Zero field splitting for S = 5/2 is not included.

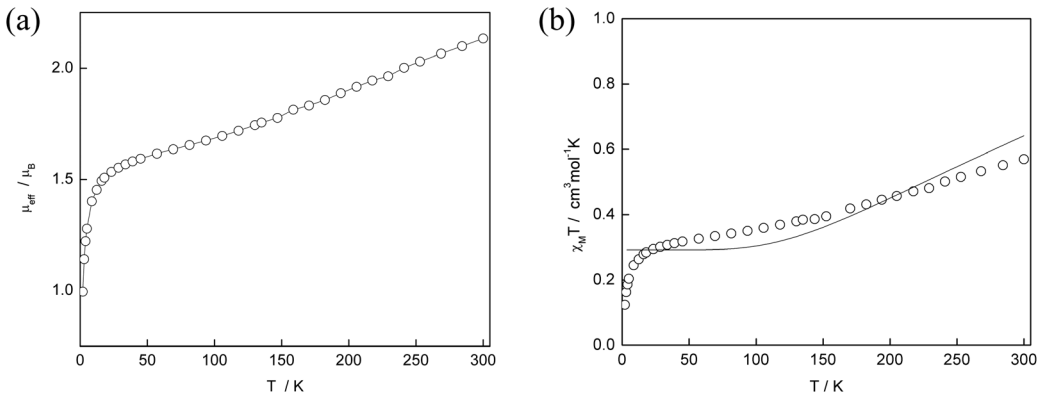

Fig. 3 Plot of (a) μ_{eff} (per two Fe centres) *vs.* *T* for **4**, in an applied field of 1 T (the solid line is a guide to the eye), and (b) $\chi_M T$ (per two Fe centres) *vs.* *T* for **4** (open circles). The solid line is that calculated for an S = 5/2 dimer model using the parameters: g = 2.0, J = –183 cm^{-1} and 3.3% monomer impurity. Zero field splitting for S = 5/2 is not included.

fraction, or (iii) weak antiferromagnetic coupling between dimers, though this seems unlikely due to the absence of any close intermolecular interactions in the crystal structure of **3**.

Use of J = –21 cm^{-1}, as determined by DFT calculations (see below), gives a fair fit between 2–50 K, with g = 2.0 and 3% monomer impurity, but the calculated 50–300 K values are much higher, with $\chi_M T$ (per two Fe centres) at 300 K determined to be *ca.* 5.0 cm^3 mol^{-1} K (μ_{eff} = *ca.* 6.3 μ_B), *i.e.* much larger than observed. Consequently, a satisfactory fit of the entire magnetic data to an S = 5/2 dimer model has not been achieved at this stage, which may, in part, be due to the co-crystallization of **3** in both its square planar (predominant) and tetrahedral (minor) forms. It is of note that the square planar coordination geometry is rare for Fe^{III} complexes, and therefore there are few available magnetic data for comparison.[10] It is also worthy of mention that efforts to fit the experimental μ_{eff} data to an intermediate spin (S = 3/2) dimer model were no more successful than those applied to the high spin (S = 5/2) dimer model.

The magnetic susceptibility data for **4** (Fig. 3(a)) are similar to those for **5** (see ESI†). An effective magnetic moment of μ_{eff} = 2.1 μ_B (per two Fe centres) was exhibited by the compound at 300 K. Both $\chi_M T$ (Fig. 3(b)) and μ_{eff} values decrease slowly from 300–20 K, with a plateau between 100–20 K, then decrease rapidly below 20 K. This is probably due to a combination of population of the S = 0 ground state and zero-field splitting of an S = 5/2 monomer impurity. A reasonable fit of the data was achieved with J = –183 cm^{-1} and g = 2.0, combined with 3.3% of an S = 5/2 monomer impurity (Fig. 3(b)). These results are in general agreement with strong antiferromagnetic coupling being present between the two Fe^{III} centres, *via* the sulfide bridges. Similar to the situation with **3**, this would explain the large divergence from the spin only value for two non-interacting h.s. iron(III) centres (*i.e.* μ_{SO} = 8.4μ_B). It is of note that the plots and calculated fit for **4** are similar to those reported by Meyer *et al.* for the unsymmetrical, anionic complex $[NEt_4]_2[\{N_2\}Fe_2(\mu\text{-}S)_2\{S_2\}]$ ($\{N_2\}$ = bis(methyl-2-indolyl)-phenylmethane,$\{S_2\}$ = *o*-xylene-α,α′-dithiolate), where g = 2.0 and J = –161 cm^{-1}, including 3.1% of monomer impurity.[16] As mentioned above, the magnetic susceptibility results for **5** are similar to those for **4**. Both $\chi_M T$ *vs.* *T* and μ_{eff} *vs.* *T* (see ESI†) decrease steadily from 300 to 20 K, then fall off sharply below

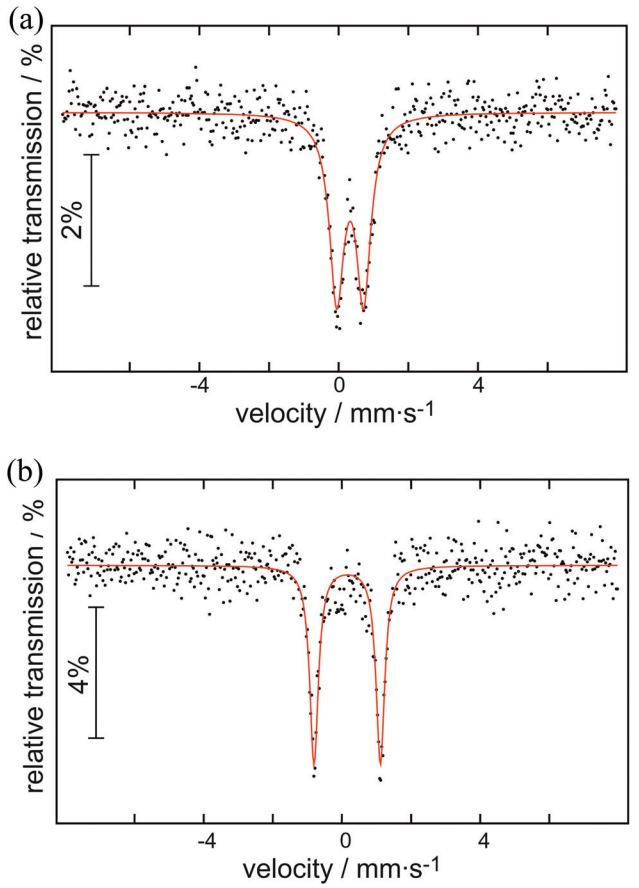

Fig. 4 Zero-field Mössbauer spectra of (a) compound **3** and (b) compound **4**, collected at 78 K. The solid lines are Lorentzian doublets fitted to the experimental values (black dots).

20 K. The effective magnetic moment (per dimer) at 300 K is *ca.* 2.2 μ_B, which is again considerably lower than the spin-only value for two h.s. iron(III) centres (see above). A reasonable fit of the data was achieved with $J = -118$ cm^{-1} and $g = 2.0$, combined with 1.0% of an $S = 5/2$ monomer impurity.

The Mössbauer spectra of doubly recrystallised samples of **3** and **4** were recorded at 78 K in a zero-field (see Fig. 4). Interestingly, the spectrum of **3** showed no evidence for the presence of a second iron species in the sample used for the experiment, despite the results of the crystallographic study. This is, however, not surprising as the counting statistics for the experiment would make the spectrum of the minor (*ca.* 8%) tetrahedral form of **3** hardly visible. The spectrum of square planar **3** exhibits a quadrupole doublet ($\Gamma = 0.51(2)$ mm s^{-1}) with a quadrupole splitting (ΔE_Q) of 0.77(3) mm s^{-1}, and an isomer shift (δ) of 0.33(2) mm s^{-1}. These values could indicate the presence of two equivalent high spin iron(III) centres in **3**. That said, the possibility that the Fe centres possess an intermediate spin ($S = 3/2$) was considered, but this was deemed unlikely as intermediate spin Fe^{III} complexes typically display significantly higher ΔE_Q values (*ca.* 3 mm s^{-1}).[10] The isomer shift for **3** is at the lower end of the range of values specifically found for five- and six-coordinate h.s. Fe^{III} dimers with a single oxo-bridge, while the quadrupole splitting is smaller than generally observed for these compounds (*i.e.* >1 mm s^{-1}).[17] Similarly, isomer shifts for cationic complexes with six-coordinate Fe$^{III}_2$(μ-O)$_2$ cores are slightly higher, while their ΔE_Q values normally lie between 1–2 mm s^{-1}.[1a,2f] These differences could be attributed to the fact that both iron sites in neutral **3** have lower coordination numbers than the Fe centres in previously reported species. A pertinent example of how abnormally low coordination at iron can affect quadrupole splittings is given by the aforementioned three-coordinate, high-spin β-diketiminato μ-oxo-diiron(II) compound [{(Nacnac)Fe}$_2$O]. The ^{57}Fe Mössbauer spectrum of this compound features δ (0.64 mm s^{-1}) and ΔE_Q (1.42 mm s^{-1}) values that could just as easily be associated with Fe^{III} centers.[8]

The Mössbauer spectrum of complex **4** exhibits a quadrupole doublet ($\Gamma = 0.30(1)$ mm s^{-1}) with $\Delta E_Q = 1.92(1)$ mm s^{-1} and $\delta = 0.15(1)$ mm s^{-1}. The isomer shift indicates the presence of two high spin iron(III) centres, and the value corresponds well with experimental data found for other complexes featuring four-coordinate h.s. Fe$^{III}_2$(μ-S)$_2$ cores.[3] It also ties in quite well with the empirical correlation, δ = 1.43–0.40 s (where s = oxidation state and δ = isomer shift), which suggests an oxidation state of +3.[3e] The quadrupole splitting is at the upper end of the range observed for these diferric systems, which might be due to the chelating guanidinate ligand causing significant distortion away from an ideal tetrahedral coordination environment in **4**. The ΔE_Q value for the compound is still considerably lower than quadrupole splittings found for all-ferrous complexes with a central Fe$^{II}_2$S$_2$ core.[3a]

DFT studies, at several theory levels, were undertaken in order to shed light on the magnetic behaviour observed for **3–5**. While the results were somewhat divergent from those obtained from experiment, calculations at the B3LYP-D2 level, carried out on the full molecules using their crystallographically determined geometries, provided the best fit with experiment. The calculations indicate that in all three complexes the Fe centres are antiferromagnetically coupled, with J values of −21.7 cm^{-1}, −237.6 cm^{-1} and −233.1 cm^{-1} for **3**, **4** and **5** respectively (using $H = -2J\mathbf{S}_1\cdot\mathbf{S}_2$ formalism). These values are at odds with the fits obtained from the experimental data, which yielded values of −145.0 cm^{-1} for **3**, −183 cm^{-1} for **4**, and −118 cm^{-1} for **5**. Although the strong antiferromagnetic coupling, suggested by experiment, for complexes **4** and **5** is broadly reproduced in our calculations, the computed J values are overestimated for these two compounds, and are severely underestimated for complex **3**.

We attempted to analyse the reason for the discrepancy between the experimental and calculated magnetic behaviour of **3**, by modelling J for the compound with its Fe centres having tetrahedral coordination environments (*viz.* **3**$_{tet}$). Calculations performed on this complex, using the geometry of the minor crystallographically characterized tetrahedral form of **3**, yielded a J value of −87.6 cm^{-1}, which indicates stronger antiferromagnetic coupling than for the square planar variant. Accordingly, it is likely that the greater than expected (based on calculations) antiferromagnetic coupling experimentally

observed for **3**, is at least in part due to co-crystallization of its square planar and tetrahedral forms. In addition, it has been reported that there is a strong magneto-structural correlation between *J* coupling values and Fe–O distances of diferric complexes containing μ-hydroxy and μ-alkoxy bridges.[18] Similarly, preliminary calculations on **3–5** show that there is a very strong dependence of *J* on both the Fe–E distances and Fe–E–Fe angles of the complexes. This dependence is strong enough that small changes in those structural parameters can lead to large changes in *J*. Consequently, it is perhaps not surprising that the correlations between the experimentally fitted and computed *J* values for **3–5** are less than ideal. A full discussion of the magneto-structural correlations for **3–5**, and related compounds, will be published elsewhere.

So as to add to our understanding of the intermetallic magnetic interactions present in **3–5**, DFT calculations were employed to determine the ground state electronic configurations of the Fe^{III} atoms in the complexes. These calculations yielded the following configurations: $[(d_{z^2})^1(d_{xz})^1(d_{yz})^1(d_{xy})^1(d_{x^2-y^2})^1]$ for **3**, $[(d_{z^2})^1(d_{yz})^1(d_{x^2-y^2})^1(d_{xy})^1(d_{xz})^1]$ for **4** and $[(d_{yz})^1(d_{z^2})^1(d_{x^2-y^2})^1(d_{xy})^1(d_{xz})^1]$ for **5** (N.B. the orbitals are arranged in order of increasing energy). Although the calculations confirm high-spin d^5 situations in each case, the orbital orderings vary significantly, as these are purely dictated by structure and the ligand donor strength. The computed molecular orbital energies and shapes for complexes **3** and **4** can be found in the ESI.†

The net magnetic exchange interaction in any given complex arises from the sum of direct exchange and super-exchange components. Although the strength of super-exchange varies with the metal ion electronic configurations and ligand field strength, the direct exchange contributions are generally correlated to the metal–metal distance in a complex. While the Fe···Fe interactions in **3–5** (*ca.* 2.47 to 2.73 Å) are most likely non-bonding in nature, they are short enough to suggest that direct exchange contributions, which arise from intermetallic d–d overlaps, are unlikely to be zero.

All of the computed overlap integral values for **3–5** are given in the ESI.† Those for complex **3** show that the strongest interaction is between the two Fe d_{yz} orbitals. As the d_{yz} orbitals are directed along the Fe–O bonds in that compound (see Fig. 5(a)), it is evident that magnetic exchange occurs predominantly *via* the oxide bridges, and is, therefore, largely super-exchange in nature. The second strongest interaction involves the Fe d_{xy} orbitals, the magnetic exchange between which is likely have both direct and super-exchange components, based upon an inspection of the molecular orbital energy level diagram for the complex (see Fig. S8 in the ESI†). The third strongest interaction is between $d_{x^2-y^2}$ orbitals and is purely super-exchange in nature. All of these interactions contribute to the moderate antiferromagnetic coupling observed for **3**.

In contrast to **3**, the most dominant Fe–Fe interactions in **4** and **5** stem from $d_{x^2-y^2}$–$d_{x^2-y^2}$ overlap (see Fig. 5(b) for the situation in **4**). In these complexes the lobes of those orbitals are directed towards each other, yielding a predominantly direct exchange interaction. Besides this, weaker d_{xy}–d_{xy} and d_{yz}–d_{yz} overlaps give rise to a super-exchange component for the complexes (see Fig. S9, ESI†). However, direct exchange dominates for the complexes, and this could lead to the very strong antiferromagnetic coupling that is apparent from the magnetic susceptibility measurements. Thus, a considerable change in magnetic behavior, from dominant super-exchange to dominant direct-exchange, is calculated for the transition from **3** to **4**/**5**.

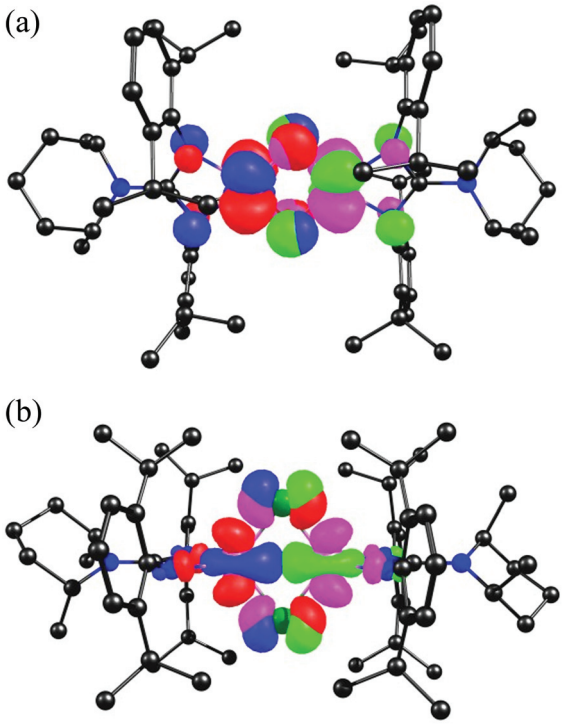

Fig. 5 Superposition of (a) the α and β d_{yz} orbitals of the iron centres of **3**, and (b) the α and β $d_{x^2-y^2}$ orbitals of the iron centres of **4**. A similar diagram for **5** can be found in the ESI.†

To probe the mechanism of coupling further, we have analysed the computed spin densities for the high-spin state of complexes **3–5** (see Fig. S11, ESI†). The spin density on each Fe^{III} centre was computed to be 4.03 for **3**, 3.84 for **4** and 3.82 for **5**. This reflects the degree of covalency of the Fe–E (E = O, S, Se) bonds, in that, as we move down the series, the Fe–E bond becomes more covalent, thus leading to a decrease in the spin density on the Fe atoms. This, in turn, leads to enhanced delocalization of the unpaired spins onto the chalcogenide ligand, and stronger antiferromagnetic coupling. It is also of note that the Fe–O bonds in **3** are largely of σ-character, while the Fe–E bonds in **4** and **5**, possess significant amounts of both σ- and π-bonding character (see Fig. S12, ESI†).

Conclusions

In summary, treatment of the metal–metal bonded iron(I) dimer [{(μ-*N*,*N*′-Pipiso)Fe}$_2$] **1**, with O_2 or N_2O, S_8 or Se_∞ led to the formation of the neutral, high-spin bis(μ-chalcogenido)-

diiron(III) complexes [{(*N*,*N*′-Pipiso)Fe(μ-E)}$_2$] (E = O **3**, S **4** or Se **5**), all of which possess central Fe$_2$(μ-E)$_2$ core structures. Compound **3** represents the first neutral, four-coordinate bis(μ-oxo) representative of this compound class, and its metal centres exhibit square planar coordination environments, which is rare for iron(III). In contrast, the iron centres in **4** and **5** possess distorted tetrahedral geometries. NMR spectroscopic, magnetic and ^{57}Fe Mössbauer spectroscopic studies indicate medium to strong antiferromagnetic coupling between the two high-spin Fe^{III} ions in all three compounds. The results of computational analyses, while not ideal, show that the unusual geometry of the bis(μ-oxo) dimer **3** sets its electronic and magnetic properties apart from those of its tetrahedral counterparts. That is, the strong magnetic coupling in complexes **4** and **5** likely stems from direct-exchange, while the moderate magnetic exchange in complex **3** is predominantly super-exchange in nature. While the discrepancy between the reported experimentally and theoretically determined magnetic properties of **3** are not fully understood at this stage, plausible explanations as to the origins of this discrepancy have been put forward. High level *ab initio* calculations on **3**, which can decompose magnetic exchange as super-exchange and direct exchange (*e.g.* CASPT2 or difference dedicated CI) may shed further light on the discrepancy, and will be investigated in due course. We continue to explore the chemistry of low-valent/low-coordinate first row transition metal complexes stabilized by extremely bulky chelating or monodentate amido ligands.

Experimental section

General methods

All manipulations were carried out using standard Schlenk and glove box techniques under an atmosphere of high purity dinitrogen. Hexane and toluene were distilled over molten potassium. ^{1}H NMR spectra were recorded on either Bruker Avance-III 400 or DPX 300 spectrometers and were referenced to the residual resonance of the solvent used (d_6-benzene). Mass spectra were obtained from the EPSRC National Mass Spectrometric Service at Swansea University. IR spectra were recorded using a Perkin-Elmer RX1 FT-IR spectrometer as Nujol mulls between NaCl plates. UV/visible spectra were recorded on a Cary 1E spectrometer in quartz cuvettes. Reproducible microanalyses for **3–5** could not be obtained, despite several attempts, because recrystallized samples of the highly air and moisture sensitive compounds were consistently contaminated by small amounts (*ca.* 8–12% as determined by integration of their ^{1}H NMR spectra) of the similarly soluble free amine (PipisoH), which could not be removed by multiple recrystallizations. Melting points were determined in sealed glass capillaries under dinitrogen and are uncorrected. Solution state effective magnetic moments were determined by the Evans method.[19] The compound [{(μ-*N*,*N*′-Pipiso)Fe}$_2$] was prepared by the literature method.[5] All other reagents were used as received.

Preparation of [{(κ^2-*N*,*N*′-Pipiso)Fe^{III}(μ-O)}$_2$] (3). [{(μ-*N*,*N*′-Pipiso)Fe}$_2$] (95 mg, 90 μmol) was dissolved in hexane (10 cm^3) and the solution cooled to −78 °C. The headspace of the reaction flask (*ca.* 50 cm^3) was purged with N_2O for *ca.* 1 minute and the flask sealed. The resultant solution was warmed to room temperature, during which time a colour change from dark red to orange-brown was observed. After stirring for a further 1.5 h, the solution was concentrated to *ca.* 3 cm^3 and stored at 5 °C for 4 h, yielding orange-brown crystals of **3**. A second crop of crystals was isolated from the mother liquor after 11 days (62 mg, 63%). M.p. = 104–110 °C; μ_{eff} (C_6D_6, Evans method) = 1.8(1)μ_B; ^{1}H NMR (300 MHz, C_6D_6, 299 K): δ = 0.22 (v.br., 24H, Dip-CH_3), 0.53 (br., 12H, Pipiso-CH_3), 0.73 (br., 6H, Pip-CH_2), 1.04, 1.20 (both br. and overlapping, 30H: 24H from Dip-CH_3, 6H from Pipiso-CH_2), 2.45 (v.br., 8H, Dip-CH(CH$_3$)$_2$), 4.73 (br., 4H, Pipiso-CHCH$_3$), 7.90 (br., 4H, Ar-*H*), 8.41 (br., 8H, Ar-*H*) ppm (tentative assignments); IR (Nujol) ν = 1614 (m), 1583 (w), 1021 (m), 934 (m), 88 (m), 796 (vs) cm^{-1}; UV-vis (toluene, 1.9 × 10^{-4} M): λ_{max}, (ε, L mol^{-1} cm^{-1}): 283 (8210), 315 (4290) shoulder tailing into the visible region; MS (EI) *m*/*z* (%): 1092.8 (M$^+$, 1), 432.3 (PipisoH$^+$-Pr^i, 100).

NB. Compound **3** can alternatively be prepared in similar yield by exposing a hexane solution of **1** to an excess of dry O_2. The workup is identical to the procedure described above.

Preparation of [{(κ^2-*N*,*N*′-Pipiso)Fe^{III}(μ-S)}$_2$] (4). S_8, (16 mg, 62 μmol) was added to a solution of [{(μ-*N*,*N*′-Pipiso)Fe}$_2$] (160 mg, 151 μmol) in toluene (25 cm^3) at −78 °C. The reaction mixture was then warmed to room temperature and stirred for 12 h, resulting in a dark brown/black solution. All volatiles were removed *in vacuo* and the residue was extracted with hexane (30 cm^3). The hexane extract was concentrated to *ca.* 15 cm^3, then placed at 5 °C for 6 days to yield dark red-brown crystals of **4** (76 mg, 45%). M.p. = 246–270 °C (decomp.); μ_{eff} (C_6D_6, Evans method) = 1.3(1)μ_B; ^{1}H NMR (400 MHz, C_6D_6, 303 K): δ = 0.97 (br., 12H, Pipiso-CH_3), 1.29, 1.48, 1.64, 1.77 (all br. and overlapping, 60H: 48H from Dip-CH_3, 12H from Pipiso-CH_2), 4.30 (br., 4H, Dip-CHCH$_3$), 4.84 (br., 4H, Ar-*H*), 5.78 (br., 8H, Pipiso-CH(CH$_3$)$_2$), 8.85 (br., 8H, Ar-*H*) ppm (tentative assignments); UV-vis (toluene, 2.5 × 10^{-4} M): λ_{max}, (ε, L mol^{-1} cm^{-1}): 353 (5080), 504 (2543), 595 (1913); IR (Nujol) ν = 1615 (s), 1584 (m), 1021 (vs), 934 (w), 866 (w), 801 (vs), 765 (w), 660 (w) cm^{-1}; MS (EI) *m*/*z* (%): 1124.7 (M$^+$, 7), 432.3 (PipisoH$^+$-Pr^i, 100).

Preparation of [{(κ^2-*N*,*N*′-Pipiso)Fe^{III}(μ-Se)}$_2$] (5). Elemental grey selenium (15 mg, 187 μmol) was added to a solution of [{(μ-*N*,*N*′-Pipiso)Fe}$_2$] (90 mg, 85 μmol) in toluene (25 cm^3) at −60 °C. The reaction mixture was slowly warmed to room temperature and stirred for 18 h, resulting in a dark brown/black solution. All volatiles were removed *in vacuo* and the residue was extracted with hexane (30 cm^3). The hexane extract was concentrated to *ca.* 15 cm^3, and placed at 5 °C for 6 days to give dark brown crystals of **5** (28 mg, 27%). M.p. > 300 °C; ^{1}H NMR (400 MHz, C_6D_6, 303 K): δ = 1.00 (br., 12H, Pipiso-CH_3), 1.61 (br., 8H, Pipiso-CH_2), 1.74 (br., 28H, Dip-CH_3 and Pipiso-CH_2 overlapping), 1.95 (br., 24H, Dip-CH_3), 3.97 (br., 4H, Pipiso-CHCH$_3$), 4.97 (br., 4H, Ar-*H*), 6.10 (br., 8H, Dip-

C*H*$(CH_3)_2$), 9.09 (br., 8H, Ar-*H*) ppm (tentative assignments); IR (Nujol) ν = 1617 (m), 1584 (w), 1022 (s), 937 (w), 799 (s) cm^{-1}; MS (EI, 8 eV) *m*/*z* (%): 1218.6 (M^+, 3), 432.3 (PipisoH$^+$-Pr, 100).

N.B. exposing d_6-benzene solutions of **5** at ambient temperature to an atmosphere of O_2 led to the essentially quantitative formation of **3**, as determined by ^{1}H NMR spectroscopy.

X-Ray crystallography

Crystals of **3–5** suitable for X-ray structural determinations were mounted in silicone oil. Crystallographic measurements on **4** were carried out at 123 K with a Bruker X8 diffractometer using a graphite monochromator and Mo Kα radiation (λ = 0.71073 Å). Crystallographic measurements on **3** and **5** were carried out at 100 K using the MX1 beamline of the Australian Synchrotron (λ = 0.7107 Å **3**, λ = 0.7108 Å **5**). The software package Blu-Ice[20] was used for synchrotron data acquisition, while the program XDS[21] was employed for synchrotron data reduction. All structures were solved by direct methods and refined on F^2 by full matrix least squares (SHELX97)[22] using all unique data. All non-hydrogen atoms are anisotropic with hydrogen atoms included in calculated positions (riding model). Crystal data, details of data collections and refinement are given in Table 2 and the ESI.† Dr Andreas Stasch (Monash University) is thanked for data collection and initial refinement of the crystal structure of **3**.

Magnetochemistry

Solid state magnetic susceptibility measurements for **3–5** were recorded over the range 300–2 K with a Quantum Design MPMS5 SQUID magnetometer using sealed quartz tubes with samples kept under an N_2 atmosphere.

Table 2 Summary of crystallographic data for compounds **3–5**

	3	**4**	**5**
Empirical formula	$C_{64}H_{96}Fe_2N_6O_2$	$C_{64}H_{96}Fe_2N_6S_2$	$C_{64}H_{96}Fe_2N_6Se_2$
Formula weight	1093.17	1125.29	1219.09
Crystal system	Triclinic	Triclinic	Triclinic
Space group	$P\bar{1}$	$P\bar{1}$	$P\bar{1}$
a (Å)	10.825(2)	10.5693(6)	10.640(2)
b (Å)	11.204(2)	11.0058(5)	11.020(2)
c (Å)	15.079(3)	15.7090(9)	15.800(3)
α (°)	93.14(3)	70.277(3)	70.48(3)
β (°)	108.64(3)	70.682(3)	70.70(3)
γ (°)	114.81(3)	69.339(3)	69.44(3)
Vol (Å^3)	1534.7(5)	1562.30(14)	1586.5(5)
Z	1	1	1
ρ (calcd) (g cm^{-3})	1.18	1.20	1.28
μ (mm^{-1})	0.52	0.57	1.65
F(000)	590	606	642
Reflections collected	15 092	20 281	30 094
Unique reflections	5169	7126	5543
R_{int}	0.0357	0.0414	0.0597
R_1 indices [$I > 2\sigma(I)$]	0.0393	0.0550	0.0313
wR_2 indices (all data)	0.0985	0.1195	0.0795
Largest peak and hole (e A^{-3})	0.55, −0.38	0.72, −0.36	0.38, −0.67
CCDC No.	1009399	1009400	1009401

Mössbauer spectroscopy

The ^{57}Fe-Mössbauer spectra of compounds **3** and **4** were recorded at 78 K in a commercial bath type cryostat in the usual transmission geometry using a ^{57}Co/Rh source. The sample was mixed with α-quartz and placed in a thin-walled PMMA container which was sealed with an epoxy resin. The isomer shift refers to α-iron at room temperature. Fitting of the spectrum was performed using the NORMOS-90 program system.[23]

Computational studies

Calculations employed the B3LYP-D2 functional, including dispersion effects as described by Grimme.[24] All calculations utilized the Alhrich triple-ζ basis set[25] as implemented in the Gaussian 09 suite of programs.[26] The *J* values were computed from the energy differences between the high spin (E_{HS}) state calculated using single determinant wave functions, and the low spin (E_{BS}) state determined using the Broken Symmetry (BS) approach developed by Noodleman.[27] Details of the computational method employed to compute the exchange interactions are discussed in detail elsewhere.[28]

Acknowledgements

This research was supported by the Australian Research Council (grant to CJ and KSM). LF thanks the Monash Institute of Graduate Research for financial support in the form of a Postgraduate Publications Award. KRV thanks the IITB-Monash Research Academy for a PhD scholarship. GR and KSM thank the Australia-India AISRF program for a research grant. The EPSRC Mass Spectrometry Service, Swansea, is also thanked. Part of this research was undertaken on the MX1 beamline at the Australian Synchrotron, Victoria, Australia.

References

1 Selected recent reviews: (*a*) L. Que Jr. and W. B. Tolman, *Angew. Chem., Int. Ed.*, 2002, **41**, 1114; (*b*) S. Friedle, E. Reisner and S. J. Lippard, *Chem. Soc. Rev.*, 2010, **39**, 2768; (*c*) L. Que Jr. and W. B. Tolman, *Nature*, 2008, **455**, 333; (*d*) E. Y. Tshuva and S. J. Lippard, *Chem. Rev.*, 2004, **104**, 987.

2 See for example: (*a*) L. H. Do, G. Xue, L. Que Jr. and S. J. Lippard, *Inorg. Chem.*, 2012, **51**, 2393; (*b*) H.-F. Hsu, Y. Dong, L. Shu, V. G. Young Jr. and L. Que Jr., *J. Am. Chem. Soc.*, 1999, **121**, 5230; (*c*) H. Zheng, Y. Zang, Y. Dong, V. G. Young Jr. and L. Que Jr., *J. Am. Chem. Soc.*, 1999, **121**, 2226; (*d*) P. J. Riggs-Gelasco, L. Shu, S. Chen, D. Burdi, B. H. Huynh, L. Que Jr. and J. Stubbe, *J. Am. Chem. Soc.*, 1998, **120**, 849; (*e*) L. S. Shu, J. C. Nesheim, K. Kaufmann, E. Münck, J. D. Lipscomb and L. Que Jr., *Science*, 1997, **275**,

515; (*f*) Y. Zang, Y. Dong and L. Que Jr., *J. Am. Chem. Soc.*, 1995, **117**, 1169; (*g*) D. Rinaldo, D. M. Philip, S. J. Lippard and R. A. Friesner, *J. Am. Chem. Soc.*, 2007, **129**, 3135.

3 See for example: (*a*) A. Albers, S. Demeshko, K. Pröpper, S. Dechert, E. Bill and F. Meyer, *J. Am. Chem. Soc.*, 2013, **135**, 1704; (*b*) A. Albers, T. Bayer, S. Demeshko, S. Dechert and F. Meyer, *Chem. – Eur. J.*, 2013, **19**, 10101; (*c*) C. T. Saouma, W. Kaminsky and J. M. Mayer, *J. Am. Chem. Soc.*, 2012, **134**, 7293; (*d*) A. Albers, S. Demeshko, S. Dechert, E. Bill, E. Bothe and F. Meyer, *Angew. Chem., Int. Ed.*, 2011, **50**, 9191; (*e*) P. V. Rao and R. H. Holm, *Chem. Rev.*, 2004, **104**, 527; (*f*) H. Beinert, R. H. Holm and E. Münk, *Science*, 1977, **277**, 653.

4 See for example: S.-B. Yu, G. C. Papaefthymiou and R. H. HolmInorg, *Chem.*, 1991, **30**, 3476.

5 L. Fohlmeister, S. Liu, C. Schulten, B. Moubaraki, A. Stasch, J. D. Cashion, K. S. Murray, L. Gagliardi and C. Jones, *Angew. Chem., Int. Ed.*, 2012, **51**, 8294.

6 L. Fohlmeister and C. Jones, *Aust. J. Chem.*, 2014, **67**, 1011.

7 C. Jones, *Coord. Chem. Rev.*, 2010, **254**, 1273; and references therein.

8 N. A. Eckert, S. Stoian, J. M. Smith, E. L. Bominaar, E. Münck and P. L. Holland, *J. Am. Chem. Soc.*, 2005, **127**, 9344.

9 J. Vela, S. Stoian, C. J. Flaschenriem, E. Münck and P. L. Holland, *J. Am. Chem. Soc.*, 2004, **126**, 4522.

10 P. J. Alonso, A. B. Arauzo, J. Fornies, M. A. Garcia-Monforte, A. Martin, J. I. Martinez, B. Menjon, C. Rillo and J. J. Saiz-Garitaonandia, *Angew. Chem., Int. Ed.*, 2006, **45**, 6707.

11 As determined by a search of the Cambridge Crystallographic Database, June, 2014.

12 B. Cordero, V. Gomez, A. E. Platero-Prats, M. Reves, J. Echeverria, E. Cremades, F. Barragan and S. Alvarez, *Dalton Trans.*, 2008, 2832.

13 See for example: (*a*) M. E. Konkle, S. K. Muellner, A. L. Schwander, M. M. Dicus, R. Pokhrel, R. D. Britt, A. B. Taylor and L. M. Hunsicker-Wang, *Biochemistry*, 2009, **48**, 9848; (*b*) S. Boxhammer, S. Glaser, A. Kühl, A. K. Wagner and C. L. Schmidt, *Biometals*, 2008, **21**, 459; (*c*) J. A. Fee, K. L. Findling, T. Yoshida, R. Hille, G. E. Tarr, D. O. Hearshen, W. R. Dunham, E. P. Day, T. A. Kent and E. Münck, *J. Biol. Chem.*, 1984, **259**, 124.

14 See for example: (*a*) J. Ballmann, X. Sun, S. Dechert, E. Bill and F. Meyer, *J. Inorg. Biochem.*, 2007, **101**, 305; (*b*) D. Coucouvanis, A. Salifoglou, M. G. Kanatzidis, A. Simopoulos and V. J. Papaefthymiou, *J. Am. Chem. Soc.*, 1984, **106**, 6081.

15 I. Raabe, K. Wagner, K. Guttsche, M. Wang, M. Grätzel, G. Santismo-Quinones and I. Krossing, *Chem. – Eur. J.*, 2009, **15**, 1966.

16 J. Ballmann, A. Albers, S. Demeshko, S. Dechert, E. Bill, E. Bothe, U. Ryde and F. Meyer, *Angew. Chem., Int. Ed.*, 2008, **47**, 9537.

17 (*a*) D. M. Kurtz, *Chem. Rev.*, 1990, **90**, 585; (*b*) K. S. Murray, *Coord. Chem. Rev.*, 1974, **12**, 1.

18 S. M. Gorun and S. J. Lippard, *Inorg. Chem.*, 1991, **30**, 1625.

19 (*a*) D. F. Evans, *J. Chem. Soc.*, 1959, 2003; (*b*) E. M. Schubert, *J. Chem. Educ.*, 1992, **69**, 62; (*c*) T. Ayers, R. Turk, C. Lane, J. Goins, D. Jameson and S. J. Slattery, *Inorg. Chim. Acta*, 2004, **357**, 202.

20 T. M. McPhillips, S. E. McPhillips, H.-J. Chiu, A. E. Cohen, A. M. Deacon, P. J. Ellis, E. Garman, A. Gonzalez, N. K. Sauter, R. P. Phizackerley, S. M. Soltis and P. Kuhn, *J. Synchrotron Radiat.*, 2002, **9**, 401.

21 W. J. Kabsch, *Appl. Crystallogr.*, 1993, **26**, 795.

22 G. M. Sheldrick, *SHELX-97*, University of Göttingen, 1997.

23 R. A. Brand, *Normos Mössbauer fitting Program*, Universität Duisburg, Duisburg (Germany), 2007.

24 (*a*) S. Grimme, J. Antony, S. Ehrlich and H. Krieg, *J. Chem. Phys.*, 2010, **132**, 154104; (*b*) S. Grimme, *J. Comput. Chem.*, 2006, **27**, 1787.

25 (*a*) A. Schafer, H. Horn and R. Ahlrichs, *J. Chem. Phys.*, 1992, **97**, 2571; (*b*) A. Schafer, C. Huber and R. Ahlrichs, *J. Chem. Phys.*, 1994, **100**, 5829.

26 M. J. Frisch, G. W. Trucks, H. B. Schlegel, G. E. Scuseria, M. A. Robb, J. R. Cheeseman, G. Scalmani, V. Barone, B. Mennucci, G. A. Petersson, H. Nakatsuji, M. Caricato, X. Li, H. P. Hratchian, A. F. Izmaylov, J. Bloino, G. Zheng, J. L. Sonnenberg, M. Hada, M. Ehara, K. Toyota, R. Fukuda, J. Hasegawa, M. Ishida, T. Nakajima, Y. Honda, O. Kitao, H. Nakai, T. Vreven, J. A. Montgomery Jr., J. E. Peralta, F. Ogliaro, M. Bearpark, J. J. Heyd, E. Brothers, K. N. Kudin, V. N. Staroverov, R. Kobayashi, J. Normand, K. Raghavachari, A. Rendell, J. C. Burant, S. S. Iyengar, J. Tomasi, M. Cossi, N. Rega, J. M. Millam, M. Klene, J. E. Knox, J. B. Cross, V. Bakken, C. Adamo, J. Jaramillo, R. Gomperts, R. E. Stratmann, O. Yazyev, A. J. Austin, R. Cammi, C. Pomelli, J. W. Ochterski, R. L. Martin, K. Morokuma, V. G. Zakrzewski, G. A. Voth, P. Salvador, J. J. Dannenberg, S. Dapprich, A. D. Daniels, O. Farkas, J. B. Foresman, J. V. Ortiz, J. Cioslowski and D. J. Fox, *Gaussian 09, Revision A.02*, Gaussian, Inc., Wallingford CT, 2009.

27 L. Noodleman, *J. Chem. Phys.*, 1981, **74**, 5737.

28 (*a*) E. Ruiz, S. Alvarez, J. Cano and P. Alemany, *J. Comput. Chem.*, 1999, **20**, 1391; (*b*) E. Ruiz, A. Rodriguez-Fortea, J. Cano, S. Alvarez and P. Alemany, *J. Comput. Chem.*, 2003, **24**, 982; (*c*) G. Rajaraman, J. Cano, E. K. Brechin and E. J. L. McInnes, *Chem. Commun.*, 2004, 1476; (*d*) P. Christian, G. Rajaraman, A. Harrison, J. J. A. McDouall, J. Raftery and R. E. P. Winpenny, *Dalton Trans.*, 2004, 2550; (*e*) G. Rajaraman, M. Murugesu, E. C. Sanudo, M. Soler, W. Wernsdorfer, M. Helliwell, C. Muryn, J. Raftery, S. J. Teat, G. Christou and E. K. Brechin, *J. Am. Chem. Soc.*, 2004, **126**, 15445; (*f*) A. Bencini and F. Totti, *Int. J. Quantum Chem.*, 2005, **101**, 819; (*g*) K. Hegetschweiler, B. Morenstern, J. Zubieta, P. J. Hagrman, N. Lima, R. Sessoli and F. Totti, *Angew. Chem., Int. Ed.*, 2004, **43**, 3436.

